

EUROPEAN ORGANIZATION FOR NUCLEAR RESEARCH

CERN/EP 86-165
21 October 1986

INCLUSIVE π^0 AND η^0 PRODUCTION IN π^-p INTERACTIONS AT 360 GeV/c

NA27 LEBC/EHS Collaboration

Aachen¹-Bombay²-Brussels³-CERN⁴-College de France⁵-Genova⁶-
Japan Universities⁷-(Chuo University, Tokyo Metropolitan University,
Tokyo University of Agriculture and Technology)-Liverpool⁸-Madrid⁹-
Mons¹⁰-Oxford¹¹-Padova¹²-Paris¹³-Roma¹⁴-Rutherford¹⁵-Rutgers¹⁶-
Serpuukhov¹⁷-Stockholm¹⁸-Strasbourg¹⁹-Tennessee²⁰-Torino²¹-Trieste²²-
Vienna²³ Collaboration

M. Aguilar-Benitez⁹, J.L. Bailly¹⁰, J.F. Baland¹⁰, S. Banerjee²,
W. Bartl²³, A.V. Batunion¹⁷, M. Begalli¹, Yu. Belokopytov¹⁷, H. Briand¹³,
R. Brun⁴, C. Caso⁶, E. Castelli²², P. Checchia¹², N. Colino⁹, R. Contri⁶,
A. de Angelis¹², L. de Billy¹³, E. Di Capua¹⁴, J. Dumarchez¹³, B. Epp²³,
S. Falciano¹⁴, C. Fernandez⁴, Yu. Fisjak¹⁷, F. Fontanelli⁶, J.R. Fry⁸,
U. Gasparini¹², S. Gentile¹⁴, R. Hamatsu⁷, L. Haupt¹⁸, S. Hellman¹⁸,
J.J. Hernandez⁴, S.O. Holmgren¹⁸, M.A. Houlden⁸, J. Hrubec²³, D. Huss¹⁹,
M. Iga⁷, M. Iori¹⁴, E. Jegham¹⁹, K.E. Johansson¹⁸, I. Josa⁹,
A. Kholodenko¹⁷, E. Kistenev¹⁷, S. Kitamura⁷, H. Leutz⁴, L. Lyons¹¹,
G. Marel¹⁴, P. Mason⁸, M. Mazzucato¹², M.E. Michalon-Mentzer¹⁹,
A. Michalon¹⁹, T. Moa¹⁸, L. Montanet⁴, G. Neuhofer²³, H.K. Nguyen¹³,
S. Nilsson¹⁸, H. Nowak⁴, G. Otter¹, G.D. Patel⁸, M. Pernicka²³,
Yu. Petrovich¹⁷, C. Pinori¹², G. Piredda¹⁴, B. Polyakov¹⁷, A. Poppleton⁴,
P. Poropat²², B. Powell⁴, S. Reucroft⁴, J. Richardson⁴, K. Roberts⁸,
H. Rohringer²³, A. Roth¹, J. Salicio⁹, M. Schouten⁴, R. Schulte¹,
B. Sellden¹⁸, M. Sessa²², S. Squarcia⁶, V. Stopchenko¹⁷, W. Struczinski¹,
K. Sudhakar², K. Takahashi⁷, M.C. Touboul¹³, U. Trevisan⁶, C. Troncon²²,
T. Tsugurai⁷, L. Ventura¹², P. Vilain³, C. Voltolini¹⁹, B. Vonck³,
B. Whymen⁸, P. Wright¹¹, T. Yamagata⁷ and G. Zumerle¹²

Submitted to Zeitschrift für Physik C

For the respective addresses see next page.

EP/3206P/LM/mk

- 1 III. Physikalisches. Inst. der Technischen Hochschule, D-5100 Aachen, Federal Republic of Germany.
- 2 Tata Institute of Fundamental Research, Bombay 400 005, India.
- 3 Vrije Univ. Brussel (VUB), B-1050 Brussel, Belgium.
- 4 CERN, European Organisation for Nuclear Research, CH-1211 Geneva 23, Switzerland.
- 5 Lab. de Physique Corpusculaire, Collège de France, F-75231 Paris Cedex 05, France.
- 6 Dipartimento di Fisica, Università di Genova, I-16146 Genova, Italy.
- 7 Tokyo University of Agriculture and Technology, High Energy Group, Koganei, Tokyo, and Tokyo Metropolitan University, Tokyo 158, Japan.
- 8 Oliver Lodge Lab., University of Liverpool, GB-Liverpool L69 3BX, England.
- 9 Grupo de Altas Energias, Junta de Energia Nuclear, E-Madrid 3, Spain.
- 10 Physique des Particules Élémentaires, Université de l'Etat à Mons, B-7000 Mons, Belgique.
- 11 Nuclear Physics Laboratory, University of Oxford, GB-Oxford OX1 3RH, England.
- 12 Dipartimento di Fisica, Università di Padova, I-35131 Padova, Italy.
- 13 Lab. de Physique Nucléaire et des Hautes Energies, Univ. Pierre et Marie Curie, F-75231 Paris Cedex 05, France.
- 14 Dipartimento di Fisica Università di Roma, "La Sapienza", I-00185 Roma, Italy.
- 15 Rutherford and Appleton Laboratory, Chilton, GB-Didcot, OX11 0QX, England.
- 16 Rutgers University, Department of Physics, New Brunswick, NJ-08903, USA.
- 17 Institut for High Energy Physics, Serpukhov, 142284 Protvino, USSR.
- 18 Institut of Physics, University of Stockholm, S-113 46 Stockholm, Sweden.
- 19 Division des Hautes Energies CRN Strasbourg and Université Louis Pasteur, B.P. 20, F-67037 Strasbourg Cedex, France.
- 20 University of Tennessee, Department of Physics and Astronomy, Knoxville, TN-37916, USA.
- 21 Istituto di Fisica, Università di Torino, I-10125 Torino, Italy.
- 22 Istituto di Fisica, Università di Trieste, I-34100 Trieste, Italy.
- 23 Institut für Hochenergiephysik der Oesterreichischen Akademie der Wissenschaften, A-1050 Wien, Austria.

ABSTRACT

The π^0 and η^0 production is studied in π^-p interactions at 360 GeV/c. The cross section for π^0 production in the forward hemisphere ($X > 0$) is $\sigma(\pi^0) = (49.7 \pm 1.0 \pm 1.1)\text{mb}$ and for η^0 with $X > 0.1$, $N_{\text{ch}} > 2$, $\sigma(\eta^0) = (3.1 \pm 0.5)\text{mb}$. The ratio of the π^0 to η^0 cross section for $X > 0.1$, $N_{\text{ch}} > 2$ is $\sigma(\pi^0)/\sigma(\eta^0) = 2.9 \pm 0.5$. Results on Feynman X and p_{T} distributions are presented. The data were obtained using the European Hybrid Spectrometer EHS and the bubble chamber LEBC at CERN.

1. INTRODUCTION

This paper is devoted to the study of the inclusive π^0 and η^0 production in π^-p interactions at 360 GeV/c. The data were collected using the European Hybrid Spectrometer (EHS) and the small rapid cycling hydrogen bubble chamber (LEBC). Fig. 1 shows the experimental set-up. A detailed description of the spectrometer is given elsewhere [1]. The photon detection was provided by two electromagnetic calorimeters: the Intermediate Gamma Detector (IGD) and Forward Gamma Detector (FGD) located 16.7 m and 41.8 m from the vertex detector respectively. The structure of the gamma detectors, the monitoring system, the calibration and shower recognition procedures are described in [2].

The inclusive approach turns out to be an interesting method for the investigation of the dynamics of multiparticle production in hadronic interactions at high energies. Pioneer work can be found in [3] where inclusive differential cross sections were first formulated, and in [4] and [5] where the scaling and limiting fragmentation hypotheses were introduced.

It should be noted that in π^-p interactions data on neutral mesons decaying into photons, at energies larger than $\sqrt{s} = 15$ GeV are scarce compared to data on inclusive charged mesons and neutral strange particle production. Note however that a similar analysis on neutral mesons produced in proton-proton interactions at $\sqrt{s} = 26$ GeV can be found in [6]. Thus a high statistics study of processes resulting in photon production at high energy, over the full range of Feynman $X > 0$ is original and interesting.

2. THE EXPERIMENTAL DATA

The present study of the π^0 and η^0 production properties in π^-p interactions at $\sqrt{s} = 26$ GeV is based on data collected during the π^- exposure of the NA27 experiment. The statistics used in this paper consists of nearly 75 000 inelastic interactions occurring in LEBC having a charged prong multiplicity $N_{ch} > 2$. This corresponds to a sensitivity of 3.7 events/ μb .

The main goal of NA27 is a detailed study of the properties and mechanisms of charm particle production in π^-p and pp interactions at 360 GeV/c and 400 GeV/c respectively. During the data taking priority was given to the collection of bias free high multiplicity data. The trigger was designed to provide a 100% efficiency for charmed events; it required at least three hits in the wire chambers W0 and W1, located directly behind the exit window of the bubble chamber (fig. 1). Thus low multiplicity and diffractive events were partially suppressed. In fig. 2 the trigger efficiency is displayed as a function of the charged prong multiplicity. The data presented in this figure are the ratios of the measured uncorrected topological cross sections to those published in [7] and taken as reference. The losses of 2-, 4- and 6-prong events are the largest ones (81%, 60% and 26%, respectively); they become relatively small for 8 and 10-prongs and negligible for higher topologies. The 2-prong events were excluded from the following analysis because they could only pass the trigger conditions due to a background of knock-on electrons or secondary interactions in the LEBC exit window.

Our "minimum bias" interaction trigger may nevertheless cause a systematic distortion of the π^0 spectra. To investigate the influence of the trigger on the 4, 6 and 8-prong events we used the Lund Monte-Carlo model [8], which describes the global features of particle-production in soft hadron-nucleon collisions reasonably well. For the purposes of this Monte-Carlo study the wire chamber efficiencies, as well as the probability for a single secondary track to imitate the multitrack configuration, were adjusted to reproduce the trigger efficiencies presented in fig. 2. The trigger efficiencies thus computed are equal to 35% and 73% for 4- and 6-prongs events respectively in reasonable agreement with the experimental values of 40% and 74% (fig. 2). The ratios of the "detected" and of the "true" π^0 spectra for these topologies computed by Monte-Carlo are presented in fig. 3. The π^0 losses are most important at large X, reflecting the kinematics of the interaction. When a leading π^0 is present in the event the charged particles have low momenta; they are mainly produced backwards in c.m.s. and miss the spectrometer acceptance. The Monte-Carlo distributions presented in fig. 3 (together with those for η^0) were fitted to polynomial functions. These were later used to correct the π^0 and η^0 spectra at the analysis stage. The correction factor thus introduced never exceeds 20% for $X < 0.90$.

3. CORRECTIONS FOR LOSSES

The gamma detectors (IGD and FGD, see fig. 1) used in this experiment operated in a high level background condition and thus a study of systematic losses is essential to reduce biases in the detection of π^0 and η^0 . A weighting procedure has to be used in order to account for these losses. In the geometry of NA27 individual photons from π^0 or η^0 decays could be lost due to the following reasons:

- γ conversion in the material of the tracking detectors and in the air.
- The geometrical acceptance of the gamma detectors.
- Cuts applied to remove low energy showers which are strongly contaminated by misidentified hadronic showers. The cuts used in this analysis are $E_{\min}(\gamma) = 0.9$ GeV for the IGD and 2.0 GeV for FGD. In fig. 4 we present the dependence of the total number of π^0 seen in the detectors (background subtracted) as function of these cuts. Lowering the cuts does not increase the signal while it increases the combinatorial background. Note that the reconstruction efficiency above the thresholds is very close to 100% for IGD but only about 20% for FGD. For the latter it reaches 100% only around $E_{\gamma} \sim 30$ GeV.
- Reduced detection efficiencies for asymmetric decays (large values of $\cos(\theta^*)$) even for the most energetic π^0 and η^0 . θ^* is the angle of the γ in the π^0 rest frame. In this paper the range of $\cos(\theta^*)$ was limited to $|\cos(\theta^*)| < 0.9$.
- The misinterpretation of two close showers as a single shower. This becomes non negligible for energetic π^0 ($E > 100$ GeV in this experiment) decaying symmetrically. The problem was solved by computing for each X-bin the $|\cos\theta^*|_{\max}$ values corresponding to a minimal reliable detectable (based upon experimental data) gamma-gamma separation and then using it explicitly in the weighting procedure.

To account for all these effects we have applied a weighting procedure based on the computation of a probability $P(X, p_T)$ for the detection and reconstruction of both photons from the decay of a particle with mass M^0 ($M^0 \rightarrow \gamma\gamma$), transverse momentum p_T and scaled longitudinal momentum X .

Considering the background conditions and imposing a reasonable limit on the weighting function $W_{\gamma\gamma}(X, p_T) = 1/P(X, p_T) < 10$, we may define the kinematic regions where it is possible to extract reliable signals of π^0 and η^0 mesons

$$\pi^0: 0.01 < X < 1.0; \quad 0.0 < p_T < 4.0 \text{ GeV}/c$$

$$\eta^0: 0.10 < X < 1.0; \quad 0.0 < p_T < 4.0 \text{ GeV}/c.$$

4. THE INCLUSIVE π^0 AND η^0 MESONS PRODUCTION

Fig. 5 shows the low mass region of the effective mass $M(\gamma\gamma)$ plotted for $X(\gamma\gamma) > 0.01$. Each combination was weighted according to $W(X, p_T) = W_{\gamma\gamma}(X, p_T) \times W_{\text{top}}$, where W_{top} is the topological microbarn equivalent; $W_{\text{top}} = \sigma_{\text{top}}/N_{\text{top}}$ (σ_{top} , N_{top} being the topological cross section and the total number of events observed with a given charged multiplicity, respectively). The experimental distribution was fitted to a gaussian plus a polynomial background of the fifth order. The fit gives a value for the π^0 mass: $M = (135.0 \pm 0.1) \text{ MeV}/c^2$ and the experimental resolution $\sigma = (8.6 \pm 0.2) \text{ MeV}/c^2$. A similar distribution for the η^0 meson mass region plotted for $X(\gamma\gamma) > 0.3$ is shown in fig. 6. The experimental resolution is $\sigma = (37 \pm 6) \text{ MeV}/c^2$.

The inclusive production cross section for π^0 meson in the events with a charged multiplicity $N_{\text{ch}} > 2$ computed from the $M(\gamma\gamma)$ effective mass distribution for $X > 0.01$ is equal to $(37.5 \pm 0.7) \text{ mb}$. The η^0 production cross section in the region $X > 0.1$ ($N_{\text{ch}} > 2$) is equal to $(3.1 \pm 0.5) \text{ mb}$ assuming a branching ratio $\eta^0 \rightarrow \gamma\gamma$ of 39% [9]. The value of the inclusive π^0 cross section in the same kinematical region is $\sigma(\pi^0, X > 0.1) = (9.0 \pm 0.5) \text{ mb}$ and the cross section ratio $\sigma(\pi^0)/\sigma(\eta^0) = (2.9 \pm 0.5)$ for $X > 0.1$ and $N_{\text{ch}} > 2$.

Using the known branching ratios for η^0 decays into final states with π^0 [9], we can estimate the contribution of η^0 mesons to the inclusive π^0 production cross section at $X > 0.1$. Using the experimental X , p_T distributions of the η^0 mesons (see below), a contribution of $(1.3 \pm 0.2) \text{ mb}$ is obtained, corresponding to about 15% of the observed π^0 production cross section for $X > 0.1$.

Fig. 7 shows the X dependence of the π^0 production in π^-p interactions at 360 GeV/c. The distribution shows a pronounced peak in the region of small X. Fitting the data in the region $0.01 < X < 0.2$ with two exponentials and extrapolating to $X = 0$ gives a value of $(11.4 \pm 0.5 \pm 1.1)$ mb for the π^0 cross section for $0 < X < 0.01$, where 1.1 contains the uncertainty of the functional behaviour of the X distribution at small X. The total inclusive cross section for π^0 production into the forward hemisphere then adds up to $(48.9 \pm 0.9 \pm 1.1)$ mb for events with $N_{ch} > 2$.

The cross sections for π^0 production as a function of charged particle multiplicity measured in our experiment, are summarized in table 1. Extrapolating from this for $N_{ch} = 2$ allows us to estimate the total inclusive π^0 cross section in the forward hemisphere: $\sigma(\pi^0) = (49.7 \pm 1.0 \pm 1.1)$ mb, $X > 0$. (The contribution $N_{ch} = 0$ is negligible at this energy).

In fig. 8 we present the average π^0 multiplicity for $X > 0$ as a function of the charged multiplicity. The cross section values for $X > 0$ are determined by the method described above. The ratio of the cross sections for forward produced π^0 to the total semi-inclusive ones (see table 1) were computed using the published data of ref. [10].

5. THE DIFFERENTIAL π^0 AND η^0 DISTRIBUTIONS

5.1 The π^0 and η^0 longitudinal momentum distributions

The invariant cross sections

$$F(X) = \int \frac{2E^*}{\pi\sqrt{S}} \frac{d^2\sigma}{dXd p_T^2} dp_T^2$$

for π^0 and η^0 production are presented in fig. 9 (E^* is the CMS energy of the meson and \sqrt{S} the total CMS energy).

The break in the slope around $X \sim 0.1$ and the sharp maximum at $X \sim 0$ which could already be seen in the noninvariant $d\sigma/dX$ cross section data (see fig. 7) are also present here.

The π^0 invariant cross section is also presented in fig. 10 for different ranges of N_{ch} . All these distributions peak at $X = 0$. In addition, a broad plateau between $X \sim 0.1$ and $X \sim 0.7$ is observed for the low charged multiplicity distributions.

Table 2 summarizes the results of the fit of inclusive π^0 and η^0 -spectra for different lower limits of the fit interval X_{min} to the power dependence

$$F(X) = A (1 - |X|)^n$$

predicted by the quark counting rules [11]. The slope value for η^0 is practically independent of the fit interval and is equal to 1.0 ± 0.3 . For the π^0 the slope slowly decreases when X_{min} is increased. At high X both distributions are characterized by the same slope in agreement with the predictions of the naive quark model. The excess of η at small X with respect to an exponential distribution can be attributed to the decay of higher mass resonances like η' and A_2 . An η' signal is observed in the $\gamma\gamma$ mass spectrum (fig. 6) and we can quote a cross section for η' , $X > 0.3$ and $N_{ch} > 2$ of 2.9 ± 1.4 mb.

The values of the slopes of the π^0 and η^0 distributions are close to the quark counting rule predictions. Therefore, one may use our results, in the $X = 1$ limit, to test various models. One of them is the dual parton model [12], which we have applied, using a version [13] which gives a good interpretation of Kp , πp and pp data up to ISR energies with a particle density $g^2 = 1.3 \pm 0.1$ in the middle of the string and a vector to pseudoscalar meson production ratio of 1.3. These two parameters can be related to the slope and the cross sections, respectively, of the π^0 and η^0 production. The results of this model are shown by the curves on fig. 9 [14]. We have used an octet-singlet mixing angle of -7° for η'/η . With this mixing angle, the model predicts $\sigma(\eta) = 2.4$ mb for $X > 0.1$ and $\sigma(\eta') = 1.2$ mb for $X > 0.3$, to be compared with our experimental results 3.1 ± 0.5 mb and 2.9 ± 1.4 mb, respectively.

5.2 The transverse momentum distributions

The p_T^2 distribution for π^0 with $X > 0.01$ is presented in fig. 11. The mean value of this distribution is $(0.20 \pm 0.01)(\text{GeV}/c)^2$ and it is clearly not exponential. It agrees well with a function of the form

$$\frac{d\sigma}{dp_T^2} = \frac{C}{(p_T^2 + \delta^2)^n}$$

with $\delta = (0.64 \pm 0.02) \text{ GeV}/c$ and $n = 4.03 \pm 0.07$. The constant in the denominator is essential for the description of the $d\sigma/dp_T^2$ distribution up to p_T values comparable with δ . In the high p_T limit the shape of the distribution is determined by the $(1/p_T^2)^n$ term. This term is usually associated with hard scattering processes taking place among hadron constituents. A value $2n = 8$ is predicted by the Constituent Interchange Model (CIM) [15] assuming that the interacting objects are $q\bar{q}$ bound systems (pions). The difference between the fitted value $2n = 8.06 \pm 0.14$ and the predicted value for hard scattering indicates that at the highest p_T accessible in our experiment, the hard scattering regime is reached.

We present in fig. 12 the transverse mass distributions of π^0 and η^0 for $x > 0.1$:

$$M_T = (M^2 + p_T^2)^{1/2} .$$

Above $M_T \sim 0.6 \text{ GeV}/c$, the two distributions are characterized by nearly the same exponential slope $(4.1 \pm 0.1)(\text{GeV}/c)^{-2}$ for π^0 and $(4.3 \pm 0.5)(\text{GeV}/c)^{-2}$ for η^0 and by similar values for the differential cross sections in this range of M_T .

6. DOUBLE DIFFERENTIAL π^0 DISTRIBUTIONS

The invariant, double differential cross sections

$$F(x, p_T^{\min}, p_T^{\max}) = \int_{p_T^{\min}}^{p_T^{\max}} \frac{2E^* d^2\sigma}{\pi\sqrt{S} dX dp_T} dp_T$$

for π^0 produced in the forward direction are presented in fig. 13 for four p_T intervals.

The low p_T distribution is characterized by the prominent peak at $X = 0$, which disappears when p_T increases. Table 3 summarizes the results of the fits of the inclusive π^0 spectrum to the power dependence $F(X) \sim (1-|X|)^n$ for the four intervals of p_T .

The observed difference in the shape of the double differential π^0 distributions for various p_T intervals indicates correlations between the π^0 transverse and longitudinal momenta. This is illustrated in fig. 14 where the $\langle p_T(\pi^0) \rangle$ dependence on X is presented. In the central region, the average transverse momentum decreases sharply down to the value of 250 MeV/c. Above $X > 0.2$, the average transverse momentum of the π^0 remains practically constant and close to 0.50 GeV/c.

7. CONCLUSIONS

In this paper we have presented high statistics data on π^0 and η^0 production in π^-p interactions at 360 GeV/c for the whole forward hemisphere over a p_T range of 0-4.0 GeV/c. The main results of the analysis are summarized below.

- (a) We have measured the total inclusive and semi inclusive π^0 and η^0 cross sections in the forward hemisphere. The inclusive cross sections are

$$\sigma(\pi^-p \rightarrow \pi^0 X; X > 0) = 49.7 \pm 1.0 \pm 1.1 \text{ mb},$$

$$\sigma(\pi^-p \rightarrow \pi^0 X; X > 0; N_{ch} > 2) = 48.9 \pm 0.9 \pm 1.1 \text{ mb}$$

$$\sigma(\pi^-p \rightarrow \eta^0 X; X > 0.1; N_{ch} > 2) = 3.1 \pm 0.5 \text{ mb}.$$

The ratio of the π^0/η^0 total cross section for $X > 0.1$ and $N_{ch} > 2$ is $\sigma(\pi^0)/\sigma(\eta^0) = 2.9 \pm 0.5$.

- (b) The inclusive and semi-inclusive π^0 and η^0 differential distributions were studied as functions of the transverse and longitudinal momenta. The slopes of the π^0 and η^0 X distributions tend to be the same at large X. The value of the exponent is close to $n \sim 1$ as predicted by the quark counting rules.
- (c) The transverse mass distributions for π^0 and η^0 mesons with $X > 0.1$ have practically the same slopes: $(4.1 \pm 0.1)(\text{GeV}/c)^{-1}$ and $(4.3 \pm 0.5)(\text{GeV}/c)^{-1}$ respectively and the corresponding differential cross sections are of a similar size.
- (d) The double differential π^0 spectra at $X \sim 1$ have slope values independent of p_T . The sharp maximum at $X = 0$ is seen only in the low p_T region.
- (e) The inclusive cross section for η' is measured to be $\sigma(\pi^- p \rightarrow \eta' x; x > 0.3; N_{ch} > 2) = 2.9 \pm 1.4 \text{ mb}$.

ACKNOWLEDGEMENTS

We wish to thank P.V. Chliapnikov, A.K. Likhoded and E.A. Kozlovsky for illuminating discussions and all the people in the various laboratories who have contributed to the construction, operation and analysis of this experiment. The support of the CERN staff operating the SPS beam and computers facilities is gratefully acknowledged as well as the organisational and typing work of Miss M. King. Financial assistance by various national funding agencies is gratefully acknowledged.

TABLE 1

Semi-inclusive π^0 cross sections, mean π^0 multiplicities and the ratio of semi-inclusive cross section for $X > 0$ to topological cross section for all X as function of charged particle multiplicity

| N_{ch} | $\sigma(\text{mb}); X > 0.01$ | $\sigma(\text{mb}); X > 0$ | $\langle n(\pi^0) \rangle; X > 0$ | $\sigma(X > 0)/\sigma[10]$ |
|----------------|-------------------------------|----------------------------|-----------------------------------|----------------------------|
| 4 | 2.45 ± 0.15 | 2.98 ± 0.16 | 1.22 ± 0.08 | 0.48 ± 0.07 |
| 6 | 4.82 ± 1.18 | 5.85 ± 0.21 | 1.81 ± 0.07 | 0.45 ± 0.05 |
| 8 | 6.72 ± 0.20 | 8.54 ± 0.29 | 2.22 ± 0.08 | 0.57 ± 0.05 |
| 10 | 6.72 ± 0.21 | 8.76 ± 0.29 | 2.55 ± 0.08 | 0.51 ± 0.05 |
| 12 | 6.05 ± 0.20 | 8.00 ± 0.31 | 3.13 ± 0.12 | 0.54 ± 0.05 |
| 14 | 4.28 ± 0.17 | 5.88 ± 0.23 | 3.59 ± 0.14 | 0.62 ± 0.07 |
| 16 | 3.14 ± 0.15 | 4.00 ± 0.21 | 4.12 ± 0.22 | 0.61 ± 0.07 |
| 18 | 1.61 ± 0.12 | 2.34 ± 0.14 | 4.54 ± 0.27 | 0.68 ± 0.11 |
| 20 | 0.70 ± 0.06 | 1.00 ± 0.07 | 4.70 ± 0.34 | |
| 22 | 0.33 ± 0.06 | 0.50 ± 0.06 | 5.69 ± 0.72 | |
| 24 | 0.11 ± 0.02 | 0.15 ± 0.03 | 4.41 ± 0.77 | |
| 26 | 0.07 ± 0.02 | 0.10 ± 0.03 | 5.47 ± 1.37 | |
| $\Sigma\sigma$ | 37.0 ± 0.5 | 48.1 ± 0.7 | 2.34 ± 0.05 | |

TABLE 2

Values of the exponent n from the fit to the differential cross section $F(X)$ of the form $(1-|X|)^{**n}$ using various values of X_{\min}

| n | $(X > 0.3)$ | $(X > 0.4)$ | $(X > 0.5)$ | $(X > 0.6)$ | $(X > 0.7)$ |
|----------|---------------|---------------|---------------|---------------|---------------|
| π^0 | 1.7 ± 0.1 | 1.5 ± 0.2 | 1.3 ± 0.2 | 1.2 ± 0.3 | 1.0 ± 0.3 |
| η^0 | 1.0 ± 0.2 | 1.0 ± 0.3 | 0.9 ± 0.3 | 0.8 ± 0.3 | 0.9 ± 0.4 |

TABLE 3

The mean value of X , together with values of exponent n from fits of the differential cross section $F(X)$ to the form $(1-|X|)^n$ for different regions of transverse momentum p_T

| p_T (GeV/c) | $\langle X \rangle$ ($X > 0.01$) | $n(X > 0.5)$ |
|---------------------|------------------------------------|---------------|
| $0.00 < p_T < 0.25$ | 0.17 ± 0.01 | 1.2 ± 0.3 |
| $0.25 < p_T < 0.40$ | 0.19 ± 0.01 | 1.3 ± 0.3 |
| $0.40 < p_T < 0.65$ | 0.20 ± 0.01 | 1.5 ± 0.3 |
| $0.65 < p_T < 1.00$ | 0.24 ± 0.01 | 1.7 ± 0.4 |

REFERENCES

- [1] M. Aguilar-Benitez et al., Zeitschr. für Phys. C31 (1986) 491.
- [2] B. Powell et al., Nucl. Instrum. and Methods 198 (1982) 217.
- [3] A.A. Logunov et al., Phys. Lett. B25 (1967) 611.
- [4] R.P. Feynman, Phys. Rev. Lett. 23 (1969) 1415.
- [5] J. Benecke et al., Phys. Rev. D5 (1969) 2159.
- [6] J.L. Bailly et al., Zeitsch. für Phys. C22 (1984) 119.
- [7] A. Firestone et al., Phys. Rev. D14 (1976) 2902.
- [8] T. Sjostrand, Comp. Phys. Comm., V27 (1982) 243.
- [9] Rev. Mod. Phys. V56, No. 2, Part II, (1984).
- [10] N.N. Biswas et al., Nucl. Phys. B167 (1980) 41.
- [11] J.F. Gunion et al., Phys. Lett. 88B (1979) 150.
- [12] A. Capella et al., Phys. Lett. 81B (1979) 68;
A.B. Kaïdalov and K.A. Ter-Martyrosyan, Sov. Journ. of Nucl. Phys. 39
(1984) 1545.
- [13] A.V. Batunion et al., Sov. Journ. of Nucl. Phys. 42 (1985) 424.
- [14] A.N. Tolstenkov, Sov. Journal of Nucl. Phys. 27 (1978) 1374;
A.K. Likhoded et al. 74.51 IHEP preprint, Serpukhov 1974.
- [15] D. Sivers et al., Phys. Rep. C1 (1976) 23.

FIGURE CAPTIONS

- Fig. 1 The version of the European Hybrid Spectrometer used for the NA27 experiment.
- Fig. 2 Trigger efficiency as function of the charged multiplicity.
- Fig. 3 Ratio of the "detected" number to "true" number of π^0 for 4, 6, 8-prongs as a function of X determined by Monte-Carlo calculations using our trigger conditions.
- Fig. 4 Number of π^0 plotted as a function of minimum accepted energy for IGD and FGD.
- Fig. 5 $\gamma\gamma$ effective mass distribution for $X > 0.01$ in the π^0 mass region.
- Fig. 6 $\gamma\gamma$ effective mass distribution for $X > 0.3$ in the η^0 mass region.
- Fig. 7 $d\sigma/dX$ distribution for the π^0 meson with results of the fit of two exponentials over the range $0.01 < X < 0.3$. In the insert, the region $x < 0.2$ is enlarged.
- Fig. 8 Mean number of π^0 ($\langle n(\pi^0) \rangle$) as a function of charged particle multiplicity.
- Fig. 9 The π^0 and η^0 invariant differential cross sections $F(X) \sim (2E^*/\pi\sqrt{S})d\sigma/dX$ as a function of X.
- Fig. 10 (a-d) π^0 semi-inclusive invariant differential cross section $F(X)$ as a function of X.
- Fig. 11 $d\sigma/dp_{T^2}$ distribution for π^0 with $X > 0.01$.
- Fig. 12 Transverse mass distribution $d\sigma/dM_T$ for π^0 and η^0 (the π^0 values have been multiplied by 10 for clarity).

FIGURE CAPTIONS

Fig. 13 (a-d) π^0 double differential cross sections $f(X, p_T)$ for the p_T intervals indicated.

Fig. 14 Mean transverse momentum $\langle p_T \rangle$ as a function of the scaled longitudinal momentum X .

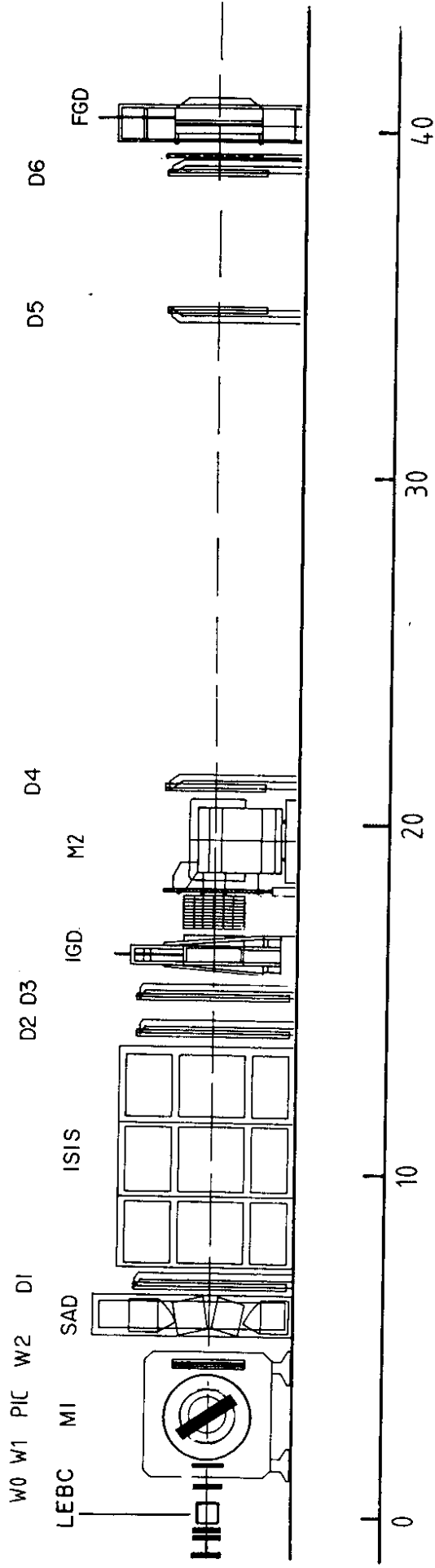


FIG. 1

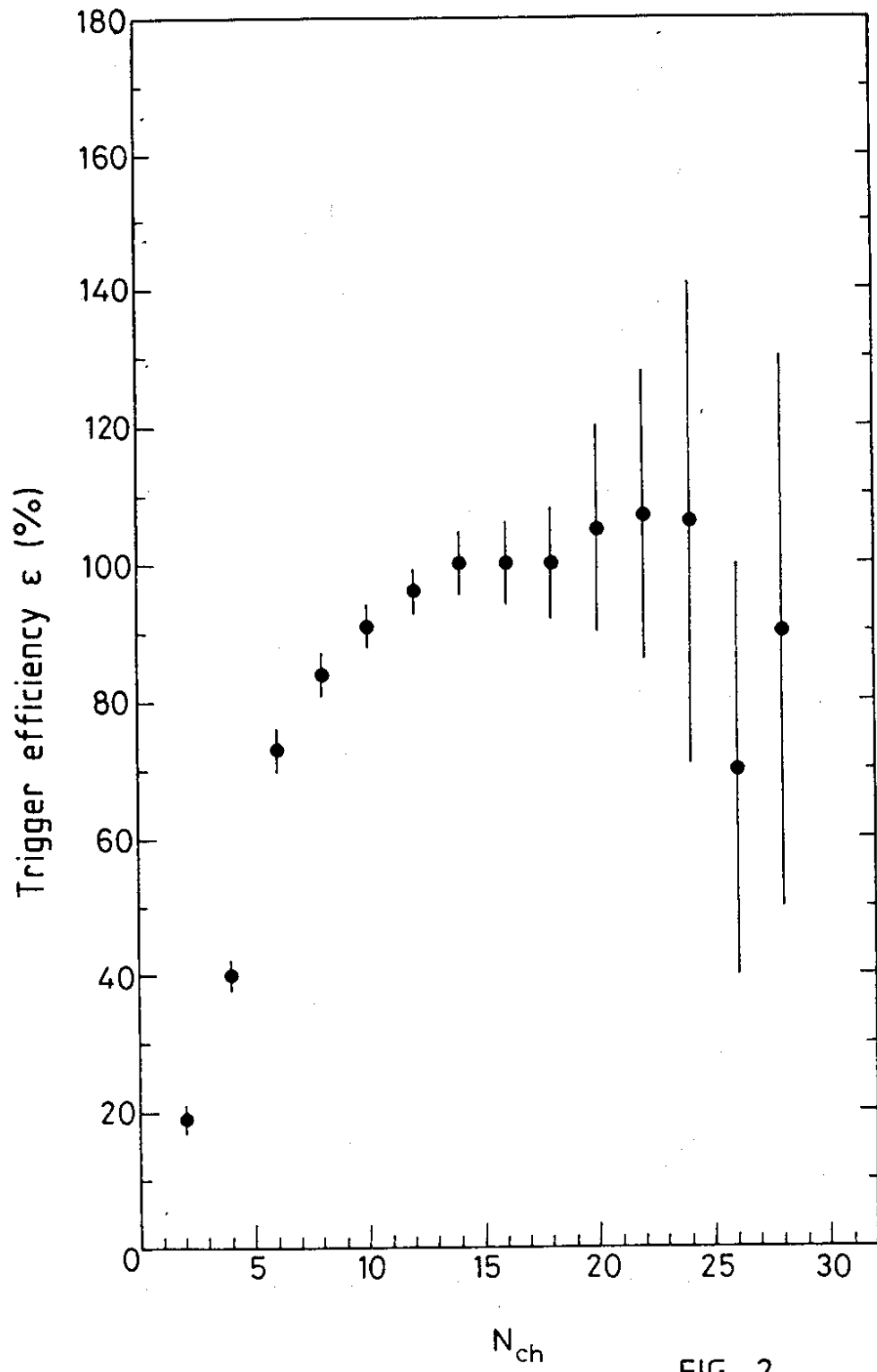


FIG. 2

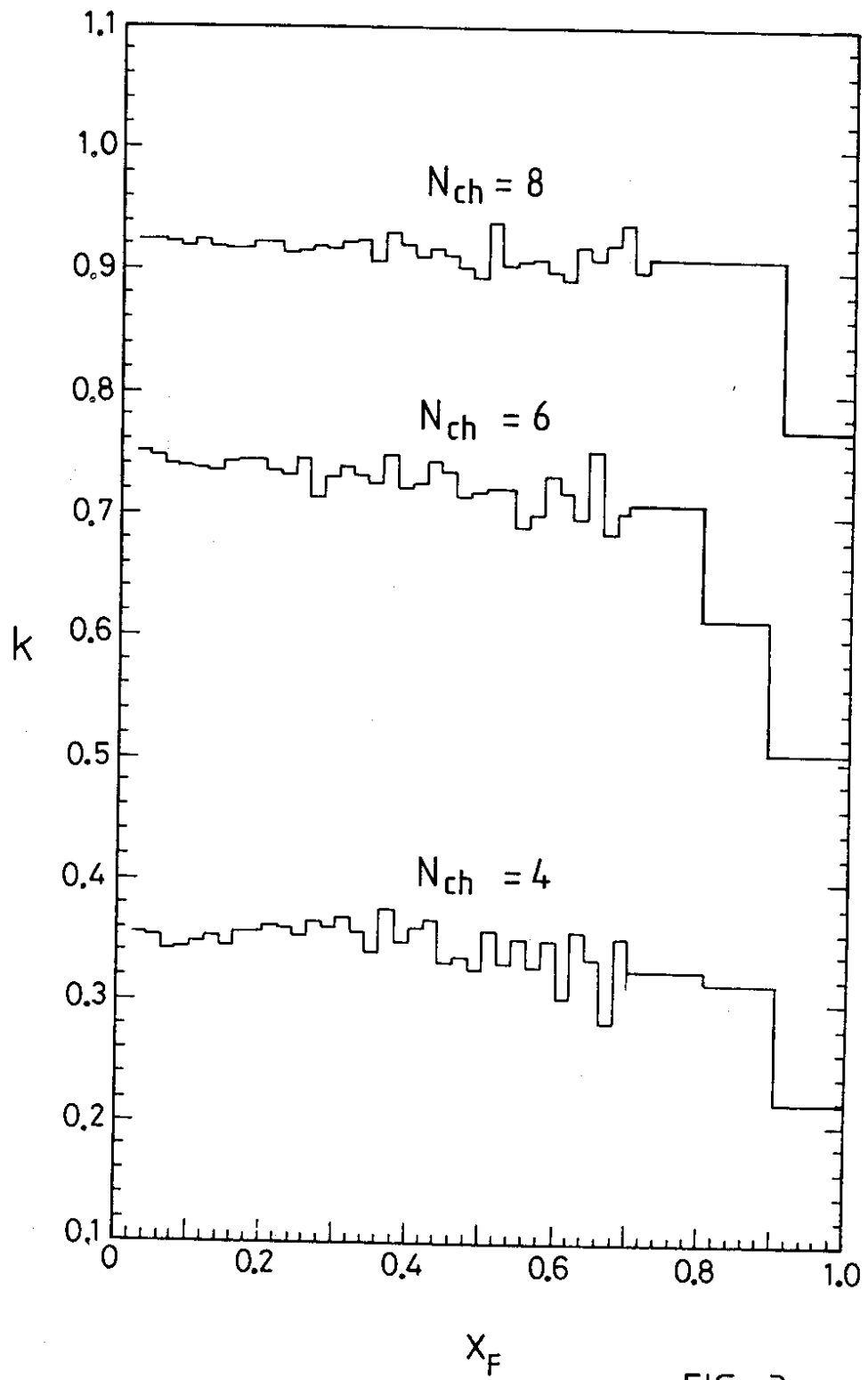


FIG. 3

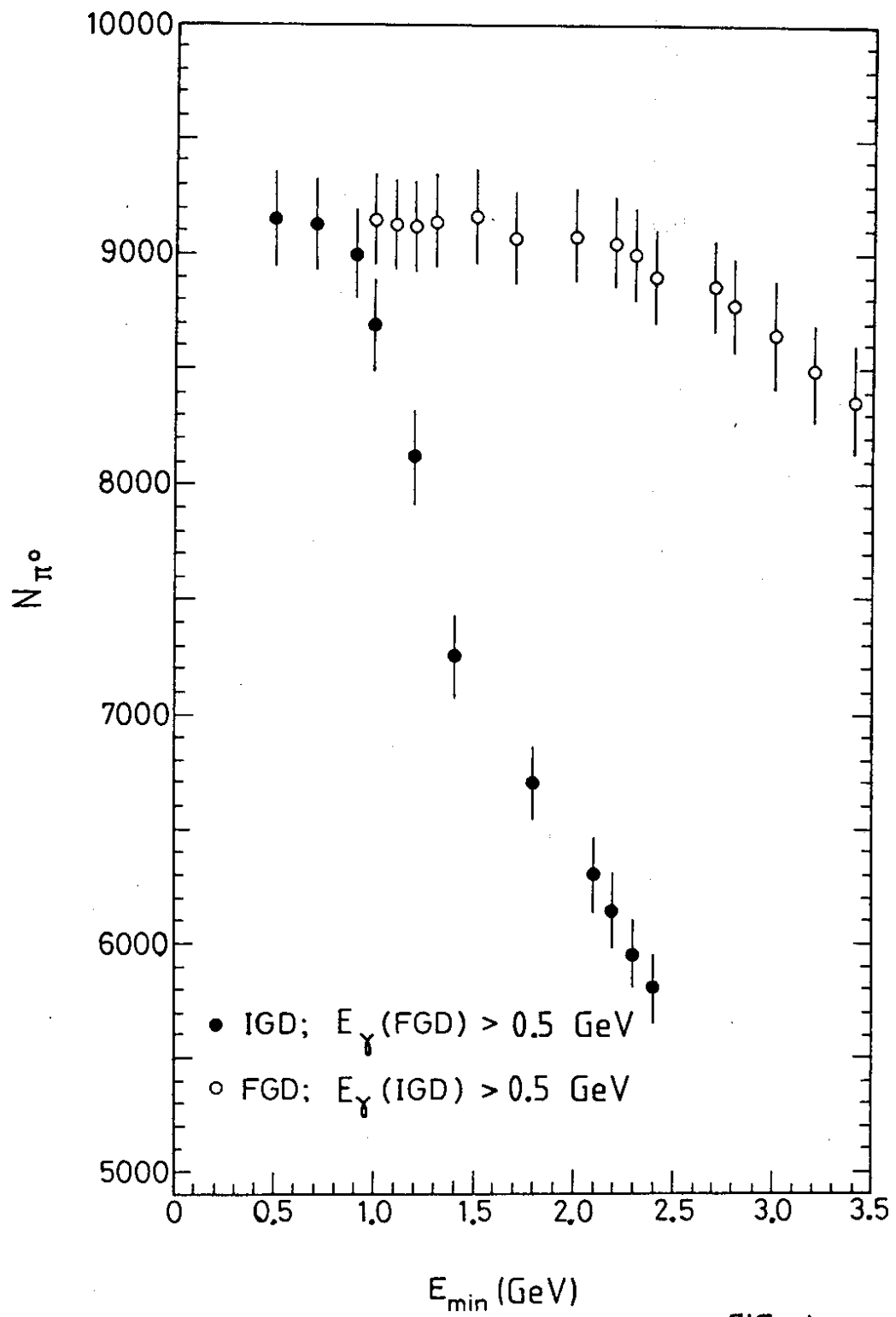


FIG. 4

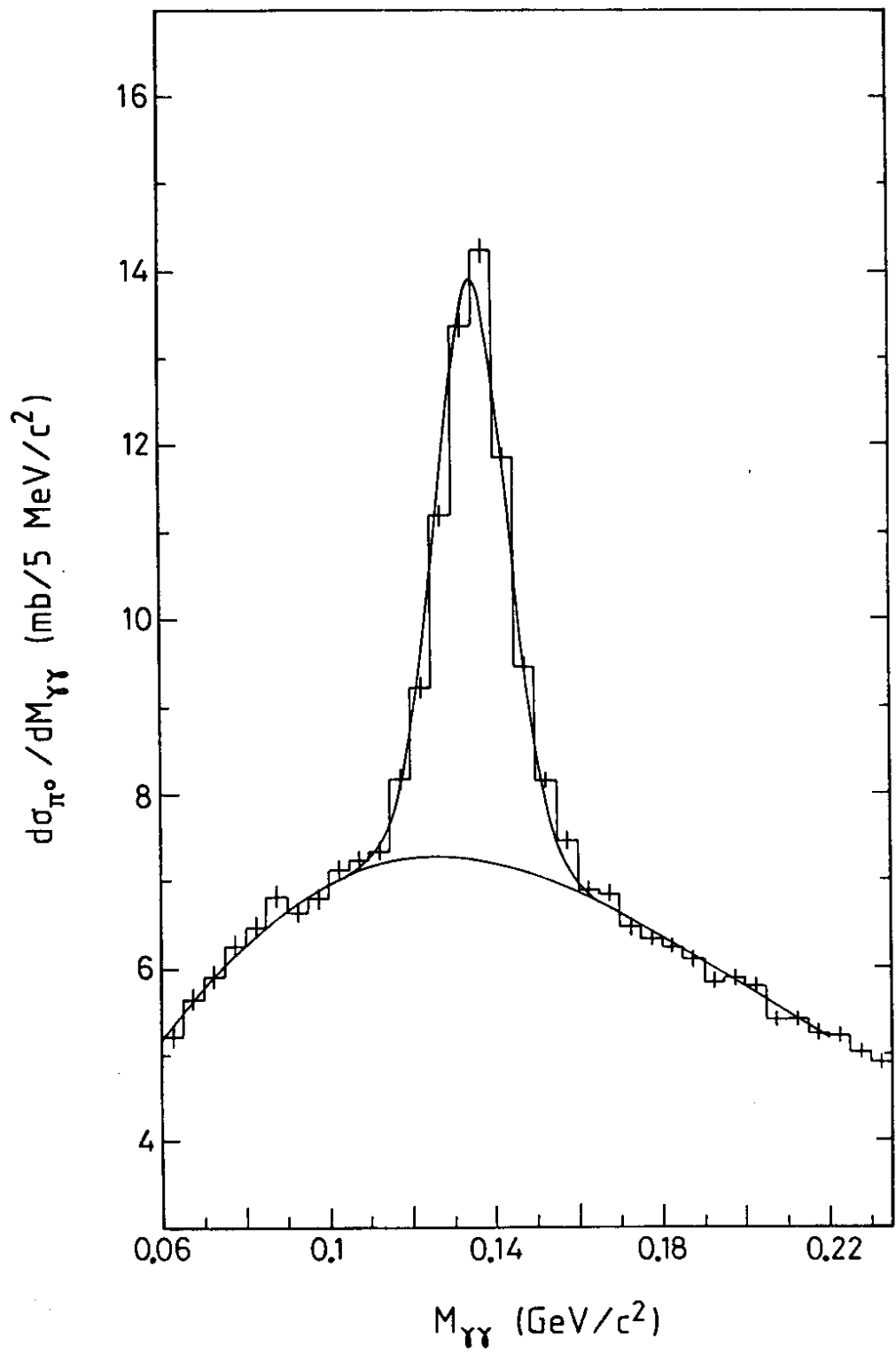


FIG. 5

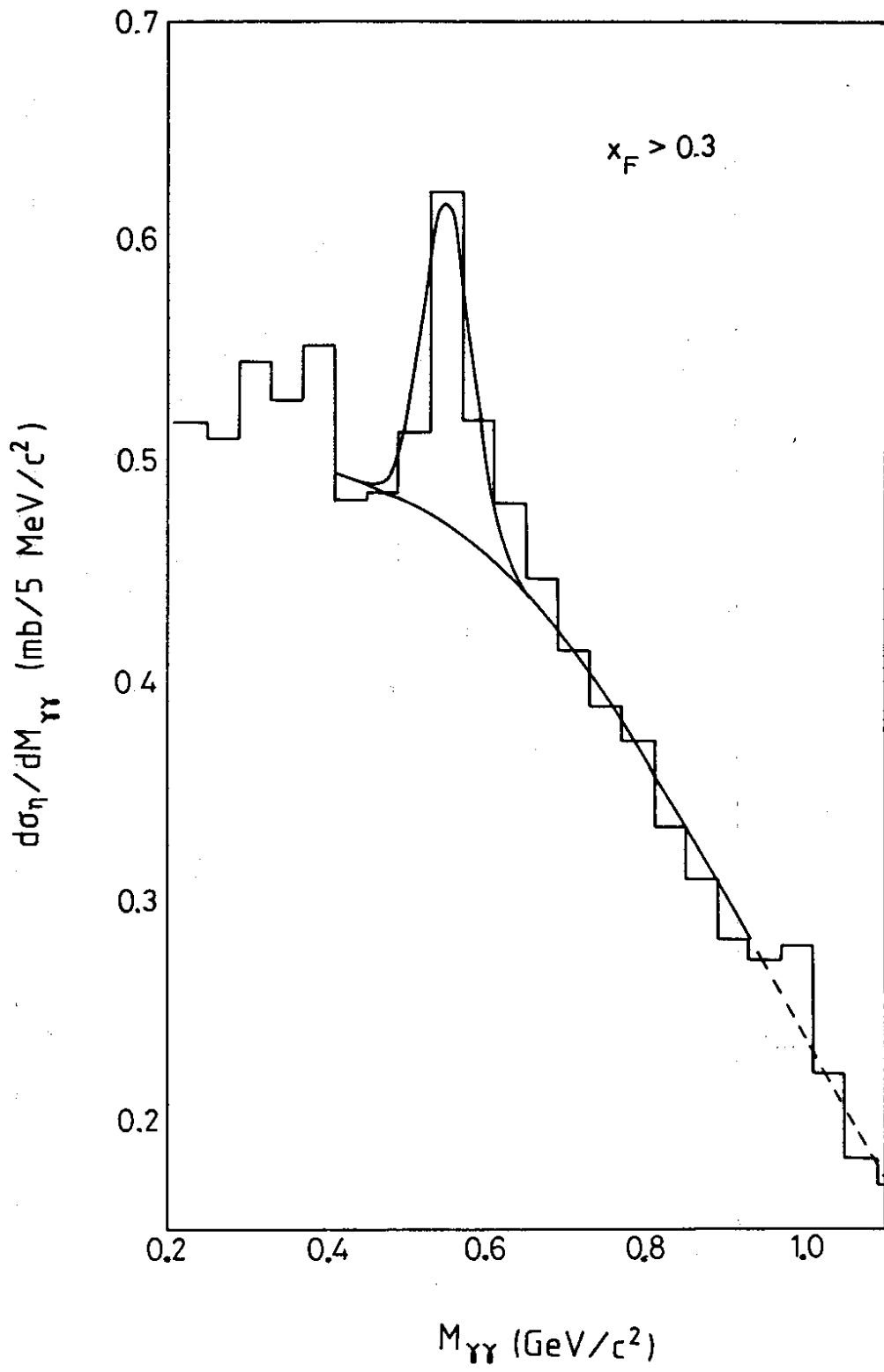


FIG. 6

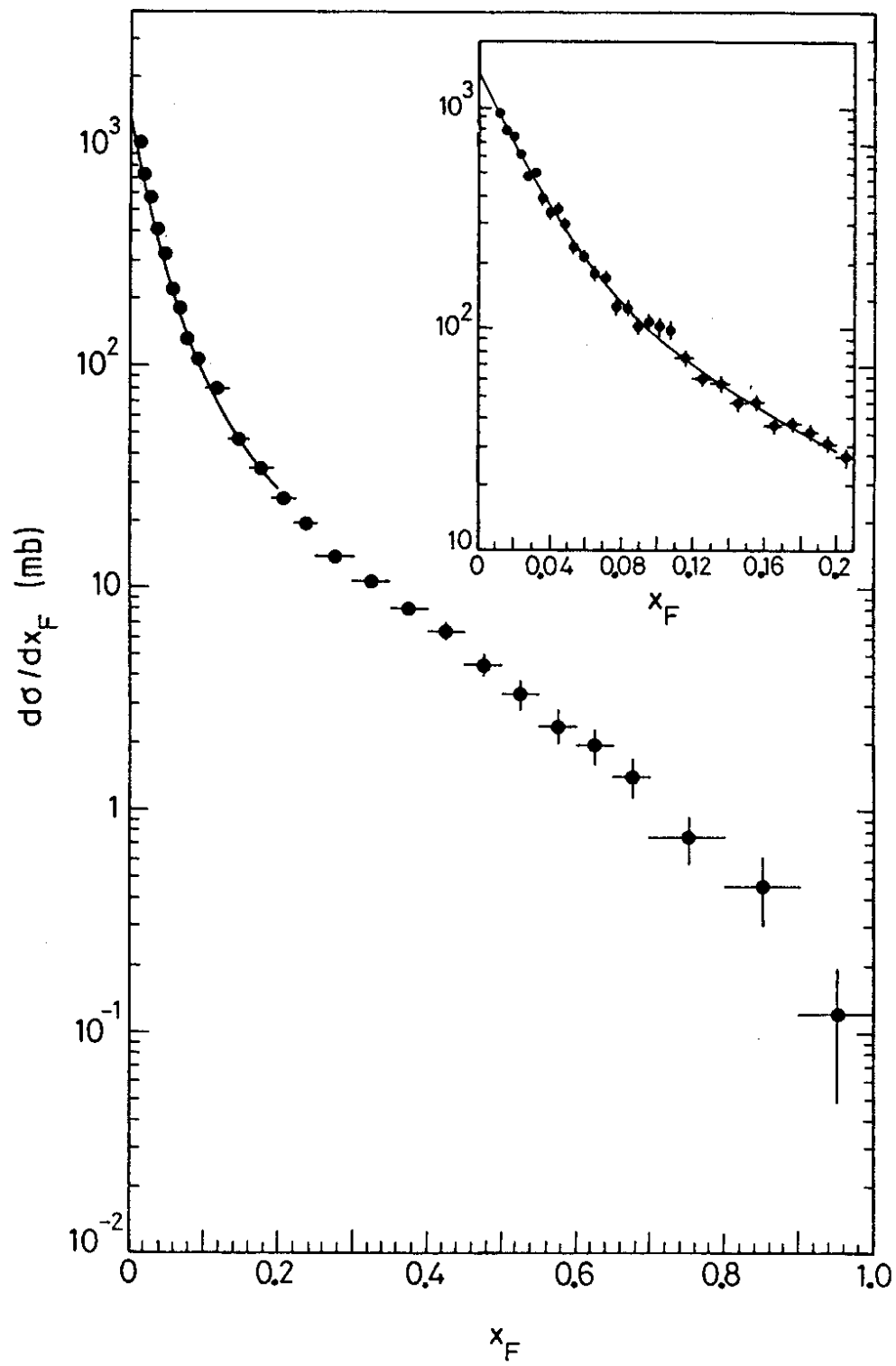


FIG. 7

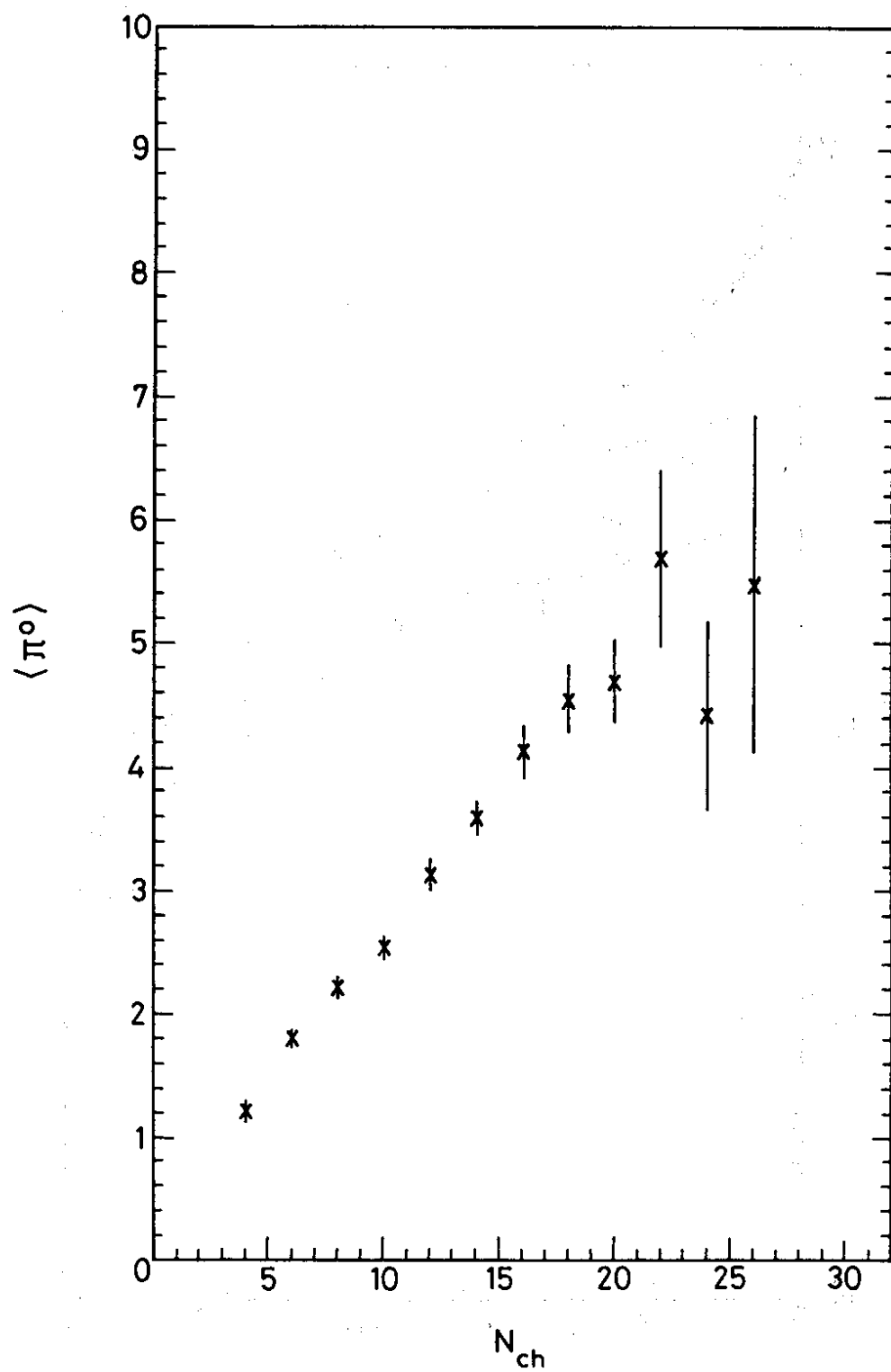


FIG. 8

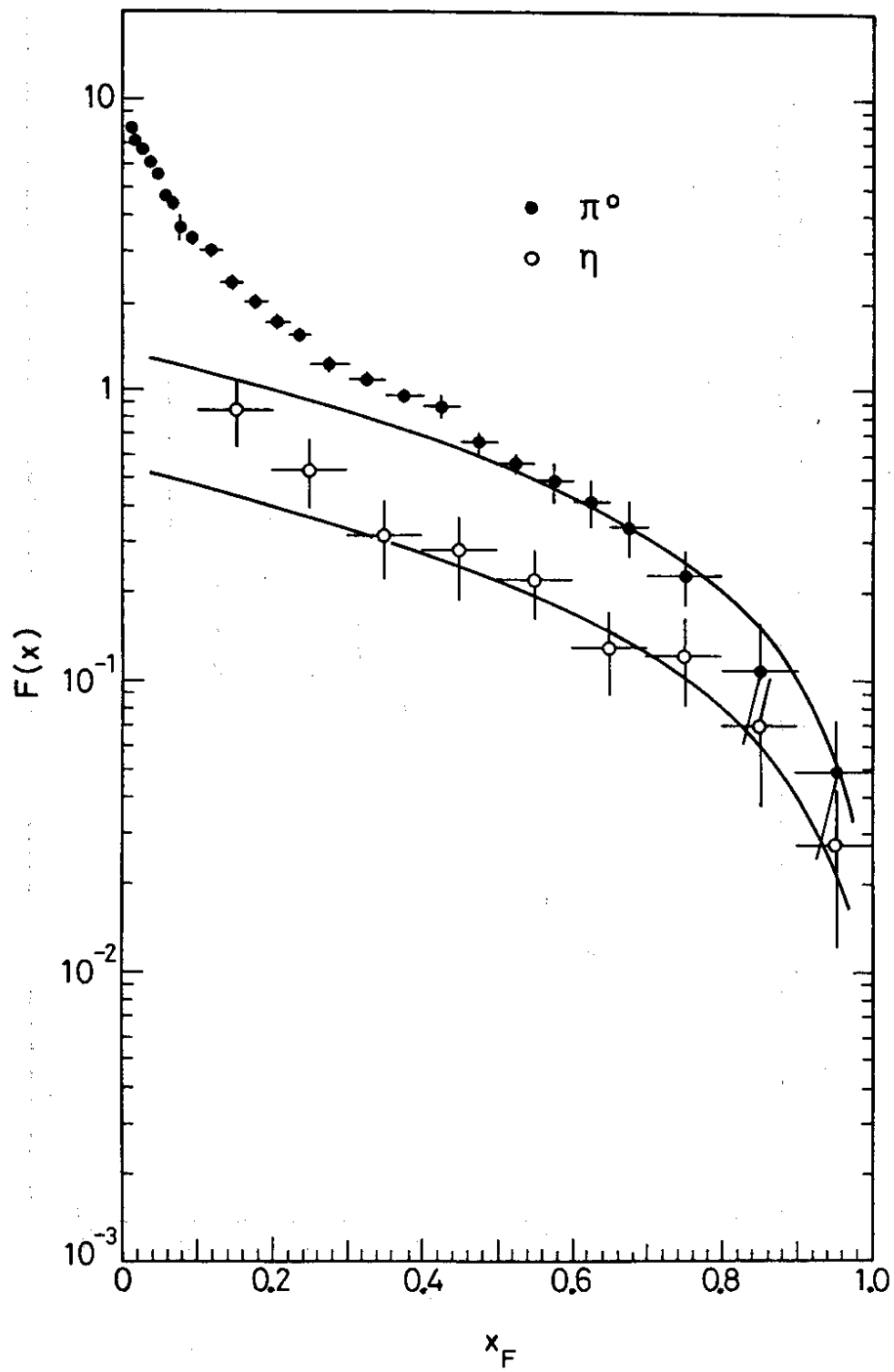


FIG. 9

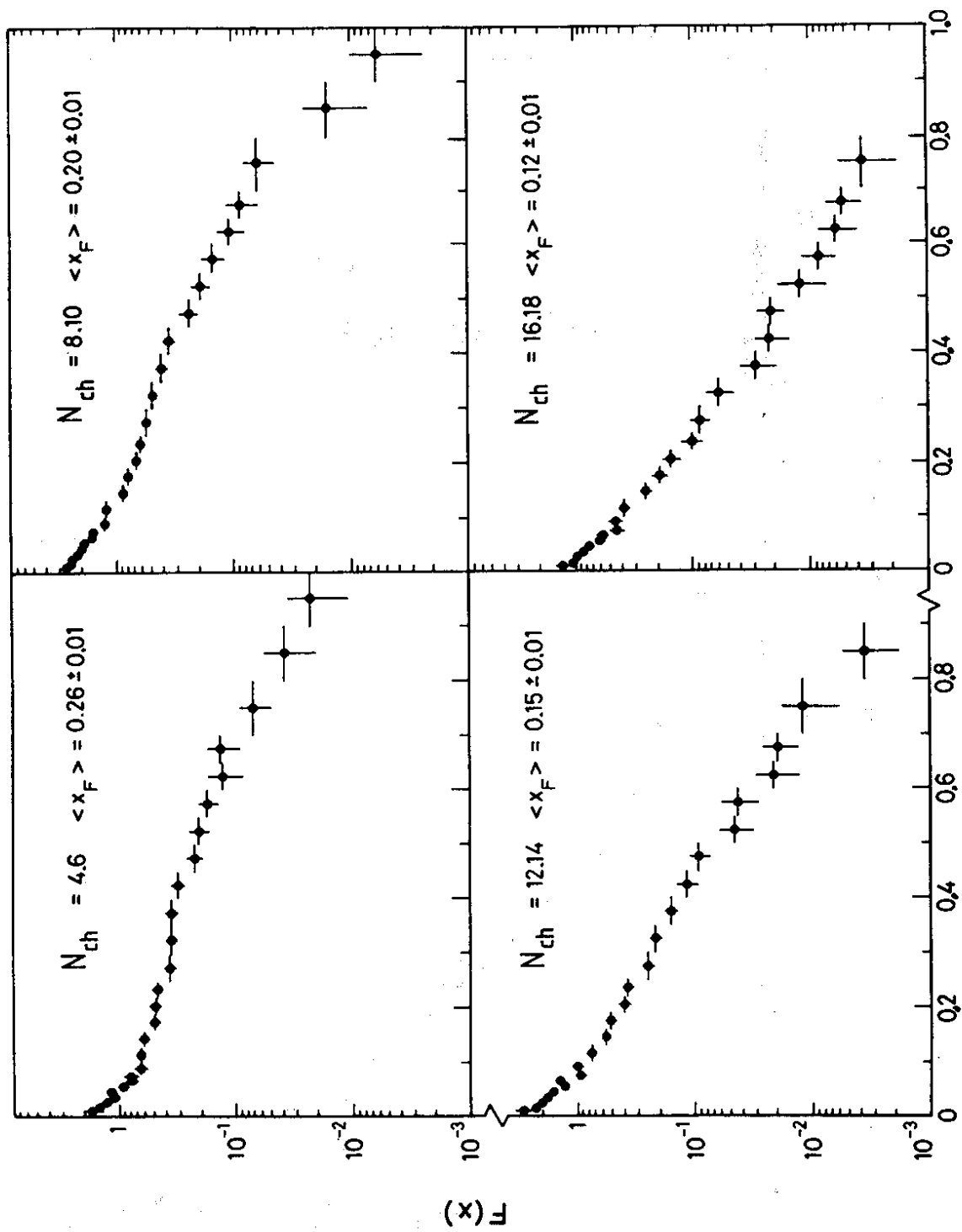


FIG. 10

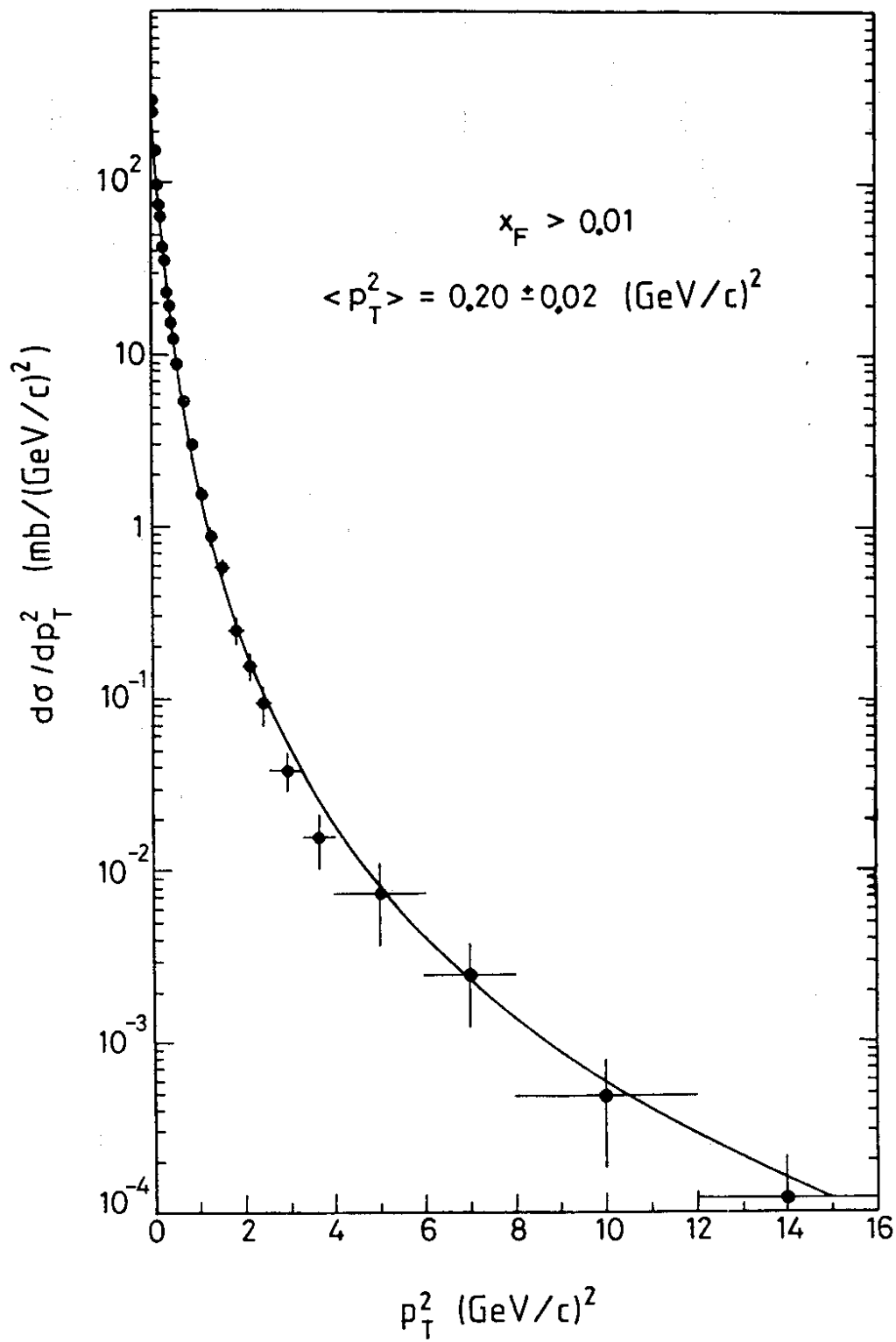


FIG. 11

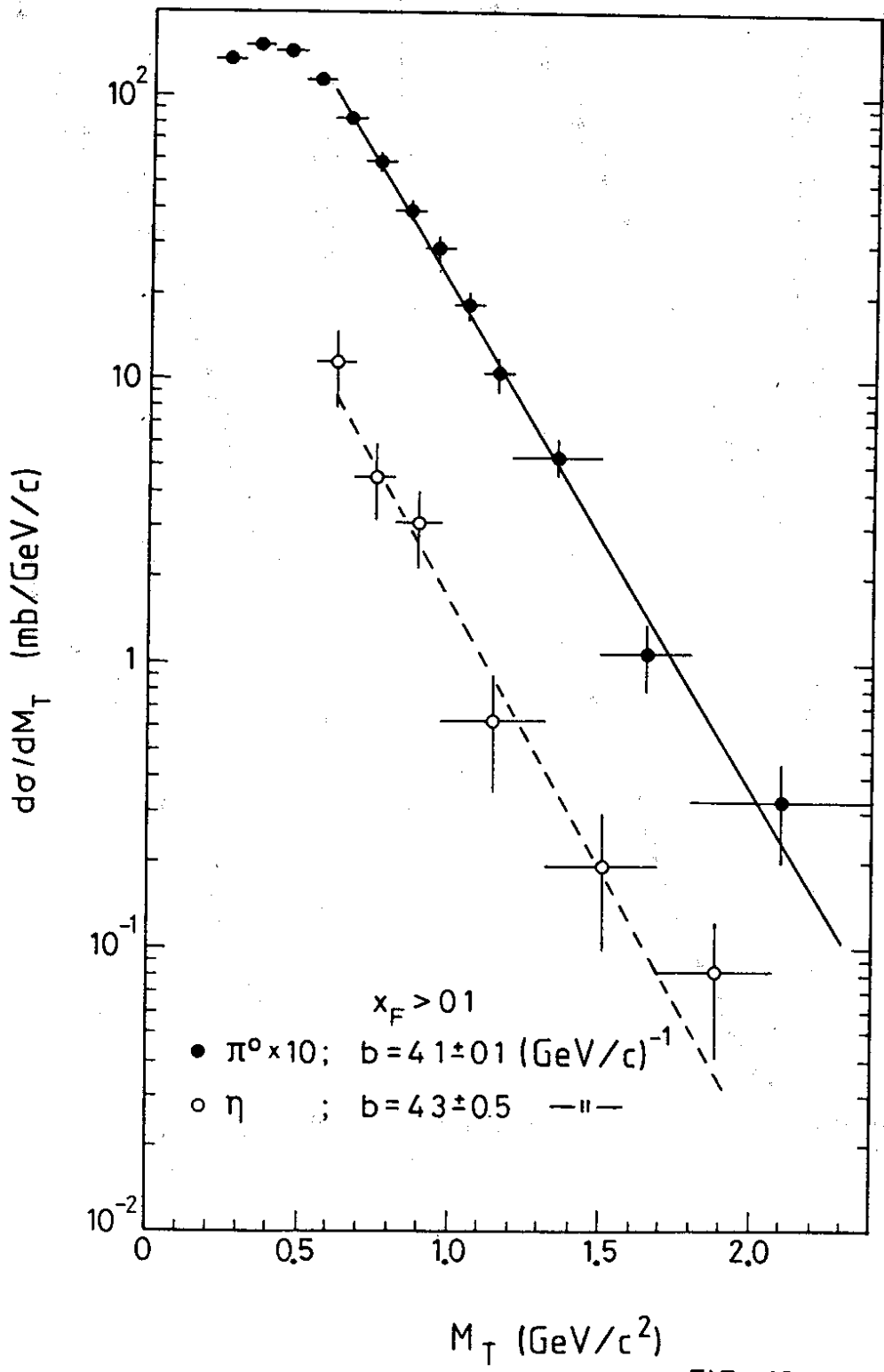
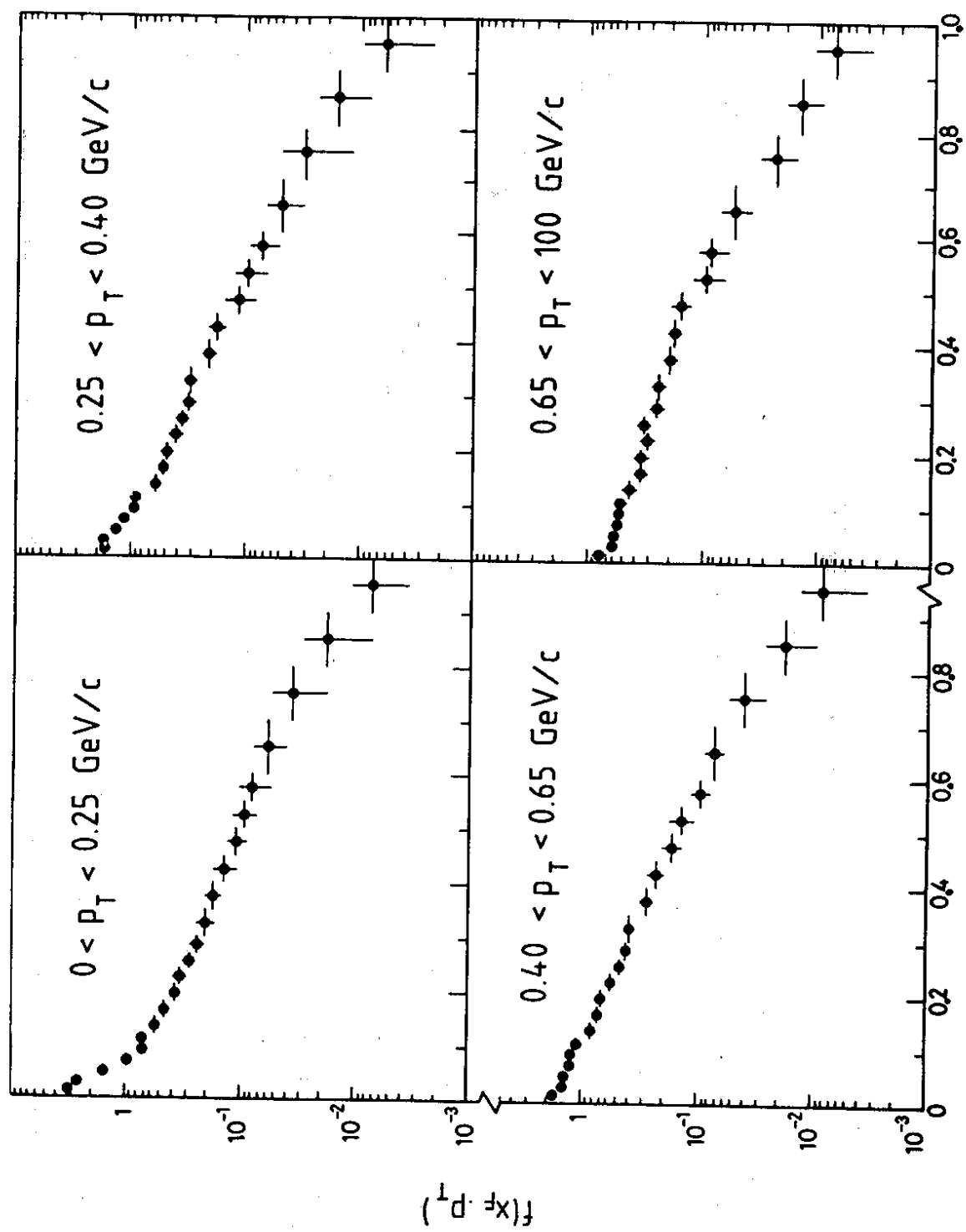


FIG. 12



X_F FIG. 13

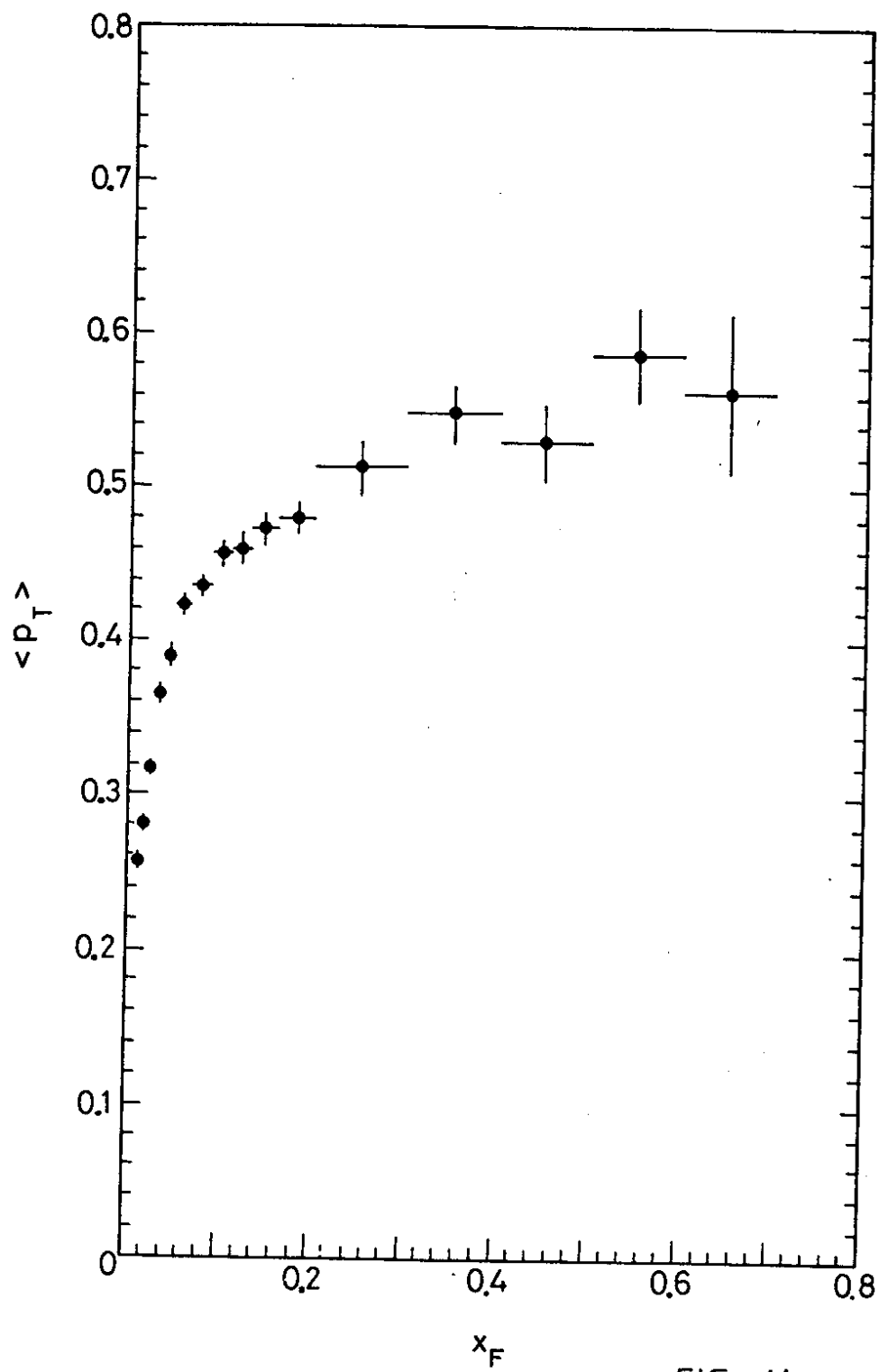


FIG. 14